Surface & Coatings Technology 258 (2014) 447–457

Contents lists available at ScienceDirect

Surface & Coatings Technology

journal homepage: www.elsevier.com/locate/surfcoat

Screening design of hard metal feedstock powders for supersonic air fuel processing

Christophe Lyphout [a,*], Katu Sato [b,1]

[a] University West, Trollhättan, Sweden
[b] Fujimi Incorporated, Japan

ARTICLE INFO

Article history:
Received 14 May 2014
Accepted in revised form 21 August 2014
Available online 7 September 2014

Keywords:
HVAF
WC-CoCr
Abrasive wear
Corrosion resistance
Carbides grain size
Design of experiment

ABSTRACT

Replacement of electrolytic hard chromium (EHC) method by Thermal Spray Technology has shown a growing interest the past decades, mainly pioneered by depositing WC-based material by conventional HVOF processes. Lower thermal energy and higher kinetic energy of sprayed particles achieved by newly-developed supersonic air fuel system, so-called HVAF-M3, significantly reduce decarburization, and increase wear and corrosion resistance properties, making HVAF-sprayed coatings attractive both economically and environmentally. In the present work, a first order process map has been intended via a full factorial design of experiments (DoE) to establish relationships between powder feedstock characteristics, such as primary carbides grain size, binder grain size and powder strength, and coating microstructure and mechanical properties. A second order process map was then established to study possible correlations between the deposit microstructural properties and their respective abrasion/erosion wear and corrosion performances.

1. Introduction

In the field of wear, erosion and corrosion applications, recent restrictions in the use of carcinogenic hexavalent form of chrome element has driven the need of replacing electrolytic hard chrome plating (EHC) by other material/process with equivalent tribological properties [1,2]. WC-based powder materials have been proposed as excellent candidates when thermally processed with high kinetic spraying systems [2,3]. Depending on the targeted industrial application, involving dry/wet abrasion/erosion wear, and associated corrosion load case, coating tribological responses to such environment has been largely investigated the past decades through the role of primary carbide grain size (CGS) of WC–Co and WC–CoCr feedstock materials [4–8]. Those studies highlighted the difficulty of minimizing carbide decarburization, being detrimental to the coating abrasion wear resistance, while spraying with air plasma spraying (APS), pulsed plasma spraying (PPS), high velocity oxy-fuel (HVOF) and activated combustion high velocity air fuel (AC-HVAF) technologies [9–14]. One of the latest low-temperature high-kinetic thermal spray processes, named as supersonic air fuel or HVAF-M3 system (UniqueCoat Technology), has since emerged as an interesting and promising alternative method to depose such temperature-sensitive material at even higher flame velocity [3]. Recent work on such HVAF–M3 system revealed the enhancement of coating tribological performances for wear and corrosion protection in the field of construction equipment and off-shore industries [15,16]. Coarsening of the CGS of initial powder feedstock was demonstrated to improve dry abrasion and erosion resistance. However the CGS appeared not to be the only powder features to explain such coating performances, but rather its ratio to the binder Grain Size (BGS), as well as the initial powder strength (PS). In the present work, a first order process map has been designed through screening objectives in order to study relationships between those factors and coating abrasion/erosion wear and corrosion performances, and to highlight the repeatability and reliability of the HVAF–M3 spraying system.

2. Experimental procedure

2.1. Feedstock materials and spray process

Pre-series commercial WC–CoCr powder feedstock materials were manufactured by Fujimi Incorporated (Japan). Ten powders, with a (−30 + 10) particle size distribution, were selected while varying their respective primary carbide grain size (CGS), binder grain size (BGS) and powder strength (PS), designated as main factors of a full-factorial design of experiments (Table 1). Domex355 coupons geometry—6 mm thick, were positioned on a rotating carousel, and coated by 15 sequential spray passes. Standard configuration of the

* Corresponding author. Tel: +46 520 223345 2.
E-mail addresses: christophe.lyphout@hv.se (C. Lyphout), satouk@fujimiinc.co.jp (K. Sato).
[1] Tel.: +81 58 379 3088.

http://dx.doi.org/10.1016/j.surfcoat.2014.08.055
0257-8972/

Table 1
Design matrix of experiments—factor levels.

Powders reference	Commercial reference	Particle size	CGS	BGS	PS	Density
		(μm)	(μm)	(μm)	(MPa)	(g/cm^3)
KB1-1[a]	DTS-W999	−30 + 5	2.0	0.5	300	3.64
KB1-2[a]	DTS-W999	−30 + 5	2.0	0.5	300	3.64
KB2	DTS-W1000	−30 + 5	0.2	0.5	100	3.82
KB3	DTS-W1001	−30 + 5	4.0	0.5	100	3.20
KB4	DTS-W1002	−30 + 5	0.2	2.0	100	3.74
KB5	DTS-W1003	−30 + 5	4.0	2.0	100	3.40
KB6	DTS-W1005	−30 + 5	0.2	0.5	500	5.30
KB7	DTS-W1006	−30 + 5	4.0	0.5	500	5.24
KB8	DTS-W1007	−30 + 5	0.2	2.0	500	4.57
KB9	DTS-W1008	−30 + 5	4.0	2.0	500	4.81
KB10	DTS-W1009	−30 + 5	0.2	2.0	300	4.04

[a] Center points of the full factorial design of experiments.

HVAF–M3 system, i.e. operating the large combustion chamber, long nozzle and short axial powder injector, was utilized for depositing the powder feedstock materials with identical spraying parameters, previously developed by the authors for such feedstock chemistry [15,16]. The HVAF–M3 system was as well utilized for gritblasting the substrates prior to deposition, utilizing mesh 220 (−75 + 45) DURALUM White F220 (Washington Mills). Microstructure features, carbide decarburization, microhardness and abrasive wear and erosion resistance of resulting coatings were evaluated as responses, including respective corrosion resistance. Weighted distributions of carbide grain size and carbide contiguity in resulting coated systems were given a particular interest, in order to correlate coatings microstructure features to wear and corrosion performances.

2.2. Statistical models

In this work, design of experiments (DoE) was used to establish relationships between WC–CoCr feedstock characteristics and HVAF–M3 sprayed coatings properties. DoE is a standard statistical approach conventionally used to study relationships between process parameters and coating properties in thermal spray. The approach is usually a stepwise procedure starting with screening fractional or full factorial designs to response surface designs for optimization purposes. In this study, a full factorial design was selected since this design can gain valuable insight in how the specific powder feedstock characteristics can interact on several responses such as coating microstructure and tribological properties. It should be noted that quantification or discretization of all factors and responses is necessary when using DoE and that the results are dependent on the selected levels of the factors (Table 1). The investigation was performed utilizing the statistical software MODDE ©, MKS Umetrics AB, Sweden. A full factorial screening design comprising 11 experimental runs in total was performed in a random order to increase the model reliability, reproducibility and repeatability, including two center points, also called *r*eplicates. Multiple linear regression (MLR) was used to establish the relationships between the factors (CGS, BGS and PS) and the selected responses. Separate MLR models were derived for each response variable, to establish a best fit for the statistical representation of the significance of each factor and their eventual interactions.

2.3. Characterization methods

2.3.1. Coating microstructure

SEM micrographs of respective coatings cross sections were analyzed utilizing a TM3000-Tabletop Microscope (HITACHI). A specially developed image thresholding algorithm utilizing the image analysis Aphelion ® software was applied on 20 SEM pictures (X7000) per samples, in order to identify volume fraction of porosity and carbide/binder phases, as well as primary carbide size and carbide contiguity weighted-distributions respectively.

2.3.2. Micro hardness Vickers

Micro-Vickers hardness measurements were carried out on the polished cross-section of the coatings according to ASTM E384-10 with a Vickers indenter at a load of 100 g, 300 g and 500 g, and a dwell time of 15 s, using a Shimadzu Microhardness Tester. Respective microhardness values were calculated from averaging series of 20 indentations, and respective distributions were analyzed via boxplot representations in order to highlight outliers.

2.3.3. Phase analysis

X-ray diffraction analysis of powder feedstock and coated systems were carried out using an D500 Siemens diffractometer, with Cr source at (35 kV/30 mA) with $\lambda - k\alpha = 0.228$ nm, in order to evaluate the carbide retention index in coated systems following reference [5].

2.3.4. Abrasive wear resistance

Suga Abrasion test was conducted according to ASTM D6037 to investigate the abrasive wear resistance of the coating. The area (30×12 mm^2) of coated systems was worn on a SiC (F180) at a reciprocating velocity of 40 DS/min, under a constant load of 30.1 N, and respective volume wear loss was evaluated.

2.3.5. Erosion wear resistance

Blast erosion test was used to investigate erosive wear resistance, where the blast material of alumina F40, a blast angle of 30°, a blast distance of 50 mm and an air pressure of 0.4 MPa were applied.

2.3.6. Corrosion resistance

Neutral salt spray test (NSS) formalized as an ASTM B117 following the ISO 9227 standard was performed to evaluate the relative corrosion resistance of coated materials exposed to a salt spray (pH 6.5–7.2) preconditioned to the operating temperature of 35 ± 2 °C and fogging a 5% salt solution at a condensate collection rate of 1.0 to 2.0 ml/h per 80 m^2. Acetic acid salt spray (ASS) was used for more corrosive environments than the ASTM B117 Standard, according to ISO 16701. A 5% by mass solution of sodium chloride in 95% of ASTM D1193 Type IV water was used and the pH was adjusted with the glacial acetic acid between 3.1 and 3.3. This solution was then atomized to create a fog that has a condensate collection rate of 1.0 to 2.0 ml/h per 80 m^2, maintaining the exposure zone to 35 ± 2 °C. Sprayed samples were grinded or polished to a Ra of 0.1, edges were protected by specially designed tape, and as-polished surface was exposed to a maximal period of 216 h (NSS) and 80 h (ASS) respectively.

3. Part I: material characterization of responses

3.1. Microstructure investigation

Powder feedstock SEM analysis preliminary shows the main difference in particle morphology between fine (0.2 μm), medium (2.0 μm) and coarse (4.0 μm) primary carbides (CGS). The role of binder grain size (BGS) and powder strength (PS) is highlighting the level of carbide distribution, anchoring and embedment (Fig. 1). The different combinations lead to a sensitive decrease of deposition efficiency while combining coarser carbide and finer binder size, an effect amplified with lower powder strength. (Fig. 2). When coarser carbide size increases above the critical splat thickness, hard phases are likely rebounding off splat [8,15], acting as an amplified erosive media processed at supersonic speed. A specially designed Image Analysis procedure utilizing Aphelion software coupled with Matlab routines has been developed to evaluate respectively coating porosity, primary carbide grain size (CGS) and contiguity (CC), distributions (Fig. 2). The analysis was performed on one cross section for each sample over 20

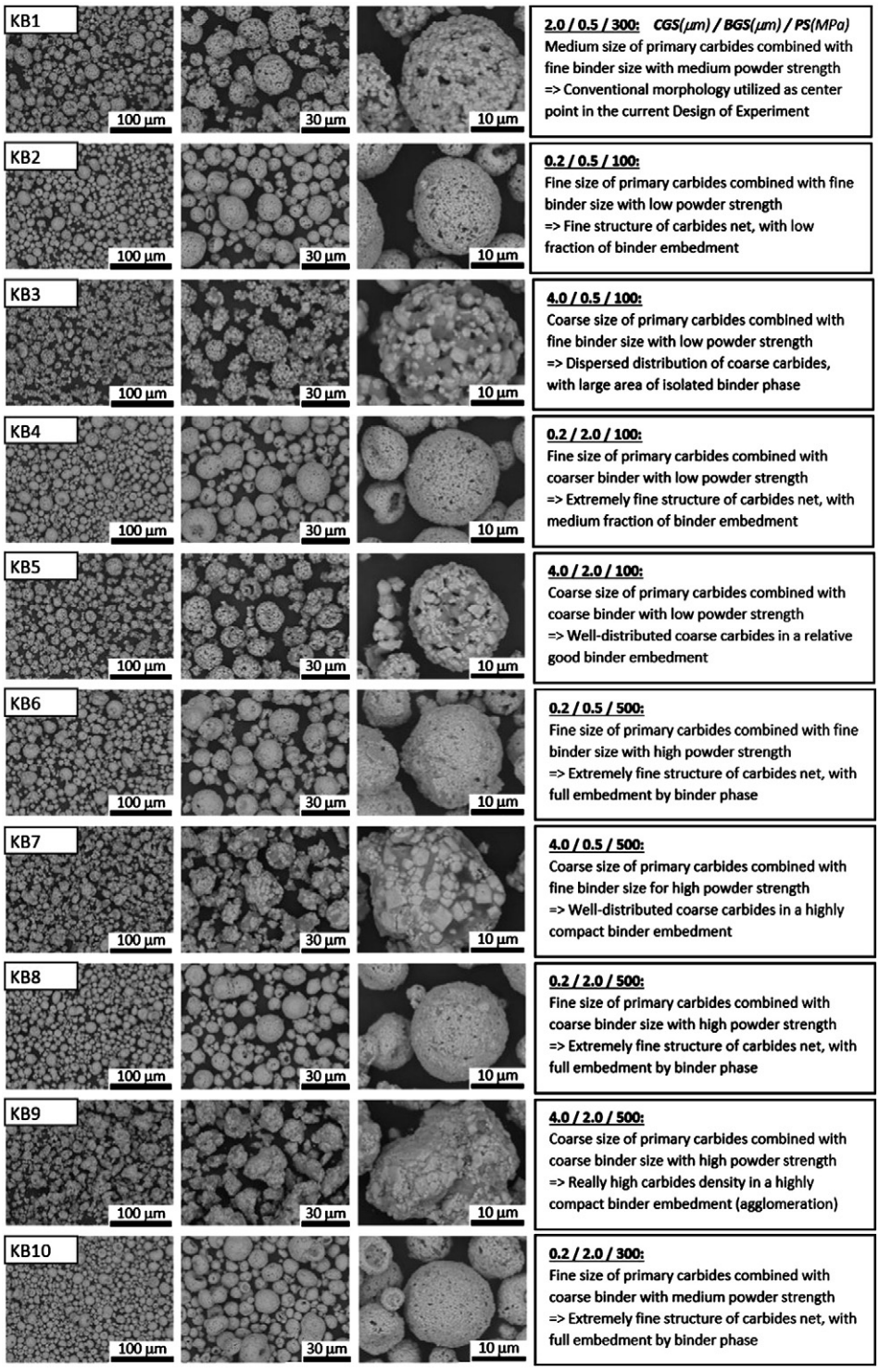

Fig. 1. SEM micrographs of respective powder feedstock materials and factor level description.

evenly distributed fields from SEM micrographs (×7000) with a dimension of 1280 × 960 pixels. Each field has been binarized by thresholding functions to identify the volume fraction of porosity, carbides and binder phases (Table 2). Each carbide contained in each field has been associated to an 'Object', described by its centroid coordinates, area, and height to width ratio. A MATLAB routine was developed to associate each object to a perfect circle with an equivalent area, in order to compute the equivalent carbide diameter distribution. Carbide contiguity was evaluated as the number-weighted mean of the length of every intercept between equivalent circles of respective carbides phase (defined as 'objects'), divided by the total carbide perimeter (Eq. (1)).

$$LCC_{ij} = \frac{\sqrt{\left((x_1)_{ij} - (x_2)_{ij}\right)^2 + \left((y_1)_{ij} - (y_2)_{ij}\right)^2}}{\Pi\left(r_i + r_j\right)} \quad (1)$$

Broad population of carbides grain size results in considering both a significant but relatively large number of small carbides that carry most

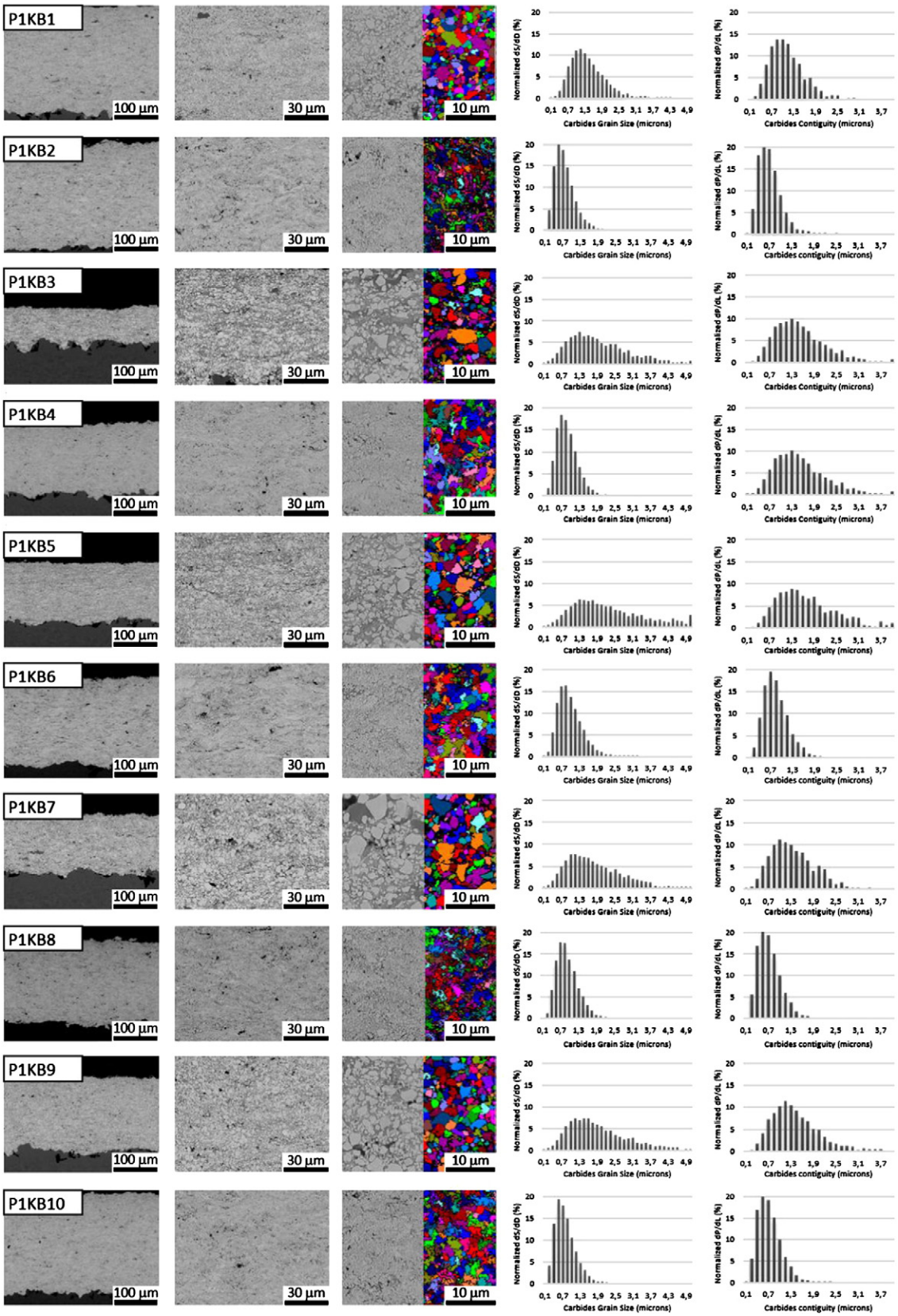

Fig. 2. SEM images and analysis of coatings carbide grain size and carbide contiguity weighted-distributions.

of the number-weighted information, and a significant but relatively small fraction of large carbides, that carry most of the area-weighted information. Therefore an area-weighted function has been applied to CGS distribution by multiplying the number-weighted distribution by the square of carbides equivalent diameter (D) (Eq. (2)). Similarly a discrete length-weighted function has been applied to the CC

Table 2
Coating microstructure evaluation by image analysis and XRD analysis for carbide retention index.

Coating reference	Volume fraction (%)			Carbide grain size distribution			Carbide contiguity distribution			Carbide retention index (%)	
	Porosity	Carbides	Binder	Weighted mean (μm)	Density (μm^{-2})	FWHM (μm)	Weighted mean (μm)	Density (μm^{-2})	FWHM (μm)	Powder	Coating
P1KB1-1[a]	1.19 ± 0.69	68.6 ± 4.86	30.2 ± 4.21	1.33 ± 0.36	1.71	1.243	1.08 ± 0.28	1.52	0.793	99	91
P1KB1-2[a]	1.31 ± 0.42	64.1 ± 3.95	34.6 ± 3.73	1.22 ± 0.31	1.92	1.122	0.97 ± 0.18	1.43	0.736	99	92
P1KB2	0.57 ± 0.27	57.1 ± 8.84	42.4 ± 6.80	0.72 ± 0.13	4.79	0.682	0.65 ± 0.10	2.66	0.459	99	70
P1KB3	0.48 ± 0.23	60.0 ± 2.30	39.5 ± 2.77	1.80 ± 0.76	1.23	2.129	1.47 ± 0.47	0.61	1.094	98	97
P1KB4	0.82 ± 0.37	70.6 ± 4.12	28.6 ± 4.45	0.84 ± 0.14	3.83	0.760	0.71 ± 0.10	3.77	0.530	99	71
P1KB5	0.72 ± 0.35	60.8 ± 2.43	38.5 ± 2.30	1.68 ± 0.68	1.42	2.034	1.29 ± 0.32	0.76	0.964	99	94
P1KB6	0.48 ± 0.30	72.7 ± 3.06	26.8 ± 3.00	0.94 ± 0.17	3.21	0.850	0.80 ± 0.12	3.47	0.611	99	93
P1KB7	1.04 ± 0.63	64.1 ± 3.42	34.9 ± 3.23	1.94 ± 0.79	0.99	2.310	1.64 ± 0.61	0.56	1.108	99	96
P1KB8	0.71 ± 0.42	64.9 ± 8.17	34.4 ± 7.93	0.75 ± 0.14	5.06	0.723	0.68 ± 0.10	3.36	0.465	99	92
P1KB9	1.04 ± 0.54	65.4 ± 4.62	33.5 ± 4.27	1.77 ± 0.71	1.24	1.939	1.38 ± 0.41	0.78	1.013	99	94
P1KB10	0.57 ± 0.27	72.3 ± 3.95	27.2 ± 3.96	0.88 ± 0.15	3.48	0.781	0.74 ± 0.10	3.74	0.556	100	82

[a] Center points of the full factorial design of experiments.

distribution by multiplying the number-weighted distribution by the respective distances relatively to the perimeters of intercepting carbides (P_{wc}) (Eq. (3)).

$$\frac{dS}{dD} = \frac{dN}{dD} D^2 \tag{2}$$

$$\frac{dP_{WC}}{dL} = \frac{dN}{dL} P_{WC} \tag{3}$$

Last but not least, it is important to specify the density of carbides (for CGS) and the density of carbide-carbide contacts (for CC), in order to emphasize not only the difference in concentrated or spread-out respective distribution between the different coatings, but also the relative concentration of the respective evaluated features. Volume fraction of porosity, carbide phase and binder phase are also presented in the following table (Table 2). Those quantitative data are here to highlight the qualitative observations made from SEM micrographs and the respective shape of CGS and CC weighted-distributions, regarding the respective original feedstock powder characteristics. The density of primary carbides and carbide–carbide contacts is here given a particular interest, as well as the broadening of that weighted-distribution with coarsening the carbides size, quantified by the full width at half maximum (FWHM). The data presented in Table 2 are at first glance difficult to be interpreted so far, but most of them present significant different values, which are about to be statistically examined within the following DoE analysis in Part II.

3.2. Carbide retention index

XRD patterns were recorded and respective phases were identified. Phases W_2C and W derived from thermal decomposition of the powder during spraying, but also thermal alteration during feedstock manufacturing process, since temperature was the most important factor in controlling the initial powder strength. Particle grain size and wettability actively played an important role in the sintering process, which might influence the respective XRD patterns. From those XRD patterns, the peaks belonging to the W_2C, W and Co_3W_3C phases also confirm some degradation of the WC particles (Fig. 3). An index of carbides retention was computed (Eq. (4)) in order to obtain a quantitative determination of the extent of decarburisation undergone by the WC–CoCr cermet [3,6]:

$$I = \frac{I_{WC}}{I_{WC} + I_{W_2C} + I_W} \tag{4}$$

where:

I_{WC} intensity of the WC peak at $2\theta = 54.1°$
I_{W2C} intensity of the W_2C peak at $2\theta = 58.4°$
I_W intensity of the W peak at $2\theta = 61.3°$

Carbide retention index was calculated for both powder and coated materials (Table 4). Carbide retention index exhibited significant differences between the different coatings, which gives a sensitive response for the following DoE analysis. Respective powder batches did not show significant difference except powder KB3 with the small amount of W element. It is interesting to notice the decarburization sensitivity of the feedstock materials to CGS, BGS and PS original variables. Fine primary carbide size combined with low particle strength leads to

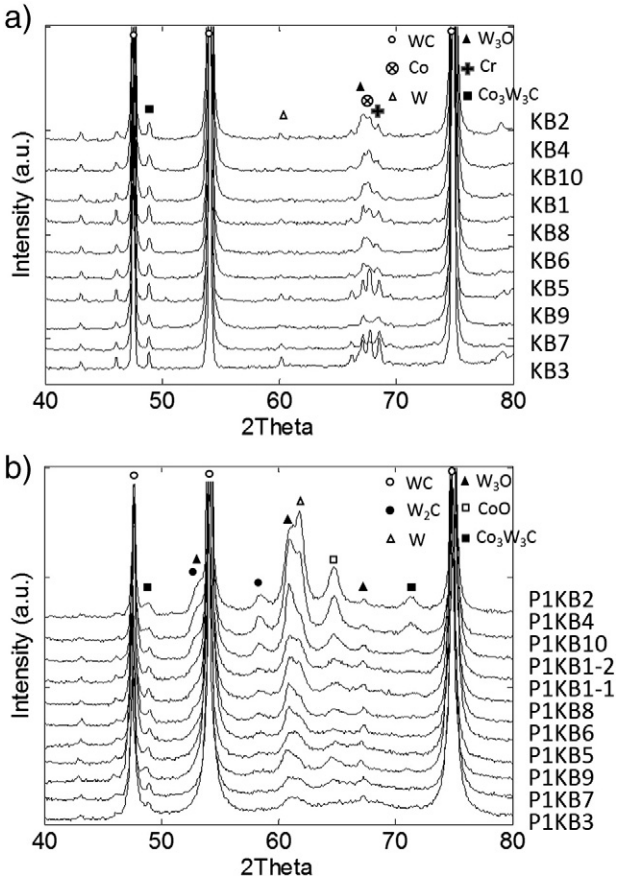

Fig. 3. XRD pattern of a) powders and b) coated systems.

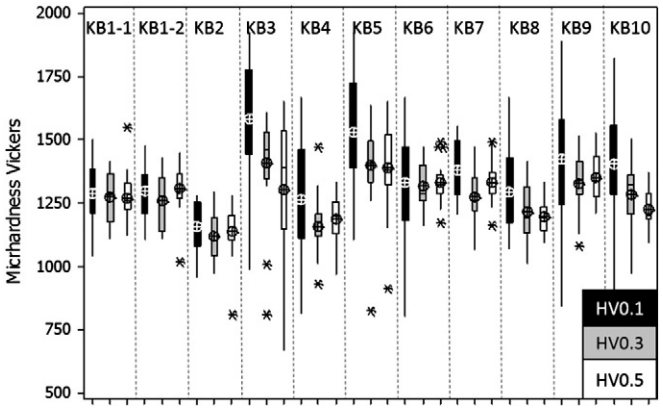

Fig. 4. Boxplot representations of coating microhardness.

higher decarburization index, in comparison to coating with coarser carbides combined with high powder strength, sprayed utilizing the present HVAF–M3 system.

3.3. Microhardness investigation

Boxplot representations of respective distributions of microhardness indentations are useful to highlight outliers' data and compute the average hardness value of the distribution, while its skewness is described by the position of the median to the quartiles. Carrying out increasing indentation loads can give a good insight of the homogenous distribution of hard phases and defects through the coating thickness. Compared to localized small indentations at low loads, higher loads are sampling an increasing gauged volume of materials and therefore the probability of including more defects statistically leads to a decrease in global micro hardness values (Fig. 4). It is therefore interesting to look at (i) how well the 20 indentations are distributed, with/without the presence of outliers here marked with a cross symbol, i.e. how well it represents the investigated population; and (ii) how large or narrow the resulting distribution is, which respectively means that the coating microstructure features are heterogenous or homogeneous. All coated systems showed a decerasing microhardness while increasing the applied indentation load, except the two center points. Coating P1KB3 and P1KB5 exhibited the highest HV0.1 above 1600, whereas P1KB2 exhibited the lowest 1200.

3.4. Abrasion and erosion wear resistance

Abrasion and erosion wear resistance of respective coatings have been evaluated. Abrasion wear loss of the two center points exhibits similar and intermediate values compared to the other coatings, which is of good promise for the next statistical modeling (Fig. 5-a). Compared to the group of P1KB3-5-7-9, the group of P1KB2-4-6-8 shows higher wear loss, mostly correlated to narrower distributions of twice finer carbide grain size and smaller carbide contiguity (Fig. 4). The highest wear loss was obtained for coating P1KB2 and P1KB4, mostly due to a high degree of decarburization which decreased respective coatings microhardness response, and consequently the abrasion wear resistance. Results from the erosion wear test did not show significant difference in volume wear losses (Fig. 5-b), except for the deposits P1BK2 and P1KB4 which showed 10% higher erosion wear losses than all the other coated systems. Comparing again the two previous groups P1KB-3-5-7-9 and P1KB2-4-6-8, the trends that both coarser CGS and broader weighted-distribution of CGS leads to improve coating wear resistance is conserved, but its significance can here be questioned for erosion wear (Fig. 5-b), compared to abrasion wear (Fig. 5-a). Each method introduces different wear mechanisms [10,16,17], involving

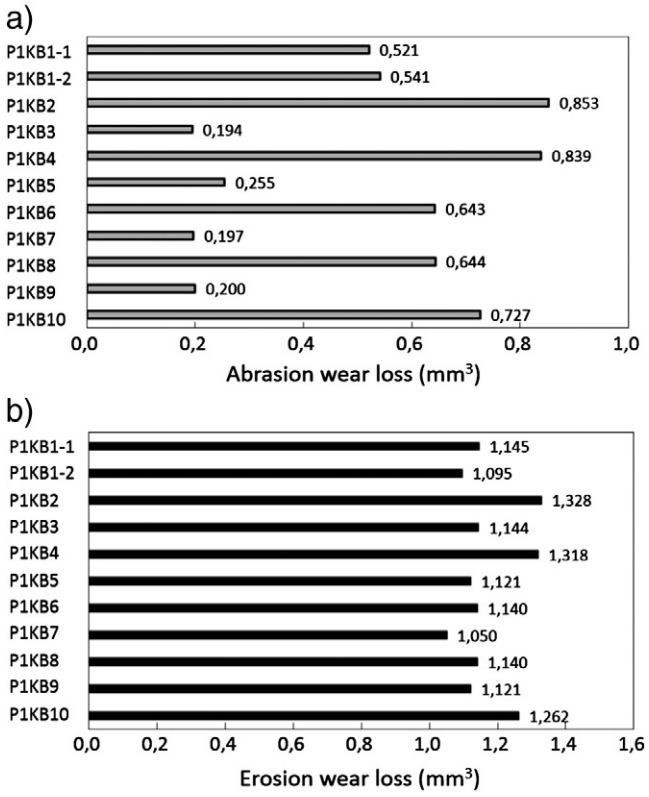

Fig. 5. Abrasion and erosion wear coating resistance.

finer (F180) SiC grit for abrasion, compared to coarser Al_20_3 (F40) for erosion blasting, which will be detailed further.

3.5. Corrosion resistance

The as-sprayed samples were previously hot mounted in Bakelite, in order to grind their surface following a standard metallographic polishing procedure (in order to follow roughness specification from the industry). Since the hot mounted resin did not seal totally the coating from its substrate on the side edge of the coated system, they were also covered by a masking tape to avoid the corrosion from the edges. Visual inspection of exposed surfaces to NSS and AASS environments was performed after 96, 144, 168 and 192 h for NSS, and after 40 and 80 h for AASS respectively (Table 3). All sprayed coatings succeeded the NSS test, except the sample P1KB9 which started to corrode after 192 h. All coatings originated from medium and coarse size of primary carbides surpassed the AASS test of 40 h (industrial

Table 3
Corrosion results for NSS and AAS environments.

Coatings reference	NSS exposure time (h)				AASS (h)	
	96	144	168	192	40	80
P1KB1-1[a]	Ok	Ok	Ok	Ok	Ok	Ok
P1KB1-2[a]	Ok	Ok	Ok	Ok	Ok	Ok
P1KB2	Ok	Ok	Ok	Ok	Failed	Failed
P1KB3	Ok	Ok	Ok	Ok	Ok	Ok
P1KB4	Ok	Ok	Ok	Ok	Failed	Failed
P1KB5	Ok	Ok	Ok	Ok	Ok	Ok
P1KB6	Ok	Ok	Ok	Ok	Failed	Failed
P1KB7	Ok	Ok	Ok	Ok	Ok	Ok
P1KB8	Ok	Ok	Ok	Ok	Failed	Failed
P1KB9	Ok	Ok	Ok	Failed	Ok	Ok
P1KB10	Ok	Ok	Ok	Ok	Failed	Failed

[a] Center points of the full factorial design of experiments.

Table 4
MLR models coefficients for selected responses.

Responses	R^2	Validity	Reproducibility	C.I.
Porosity	0.144	0.563	0.918	95%
Carbide vol.	0.608	0.827	0.573	95%
Binder vol.	0.516	0.896	0.016	95%
CGS	0.979	0.874	0.973	95%
CC	0.959	0.856	0.953	95%
CGS—density	0.965	0.520	0.991	95%
CC—density	0.954	0.490	0.998	95%
CGS—FWHM	0.958	0.762	0.983	95%
CC—FWHM	0.953	0.792	0.975	95%
HV0.3	0.903	0.567	0.990	95%
I-WC	0.987	0.949	1	95%
Abrasion wear	0.993	0.735	0.997	95%
Erosion wear	0.904	0.869	0.848	95%
Corrosion NSS	0.444	−0.200	1	95%
Corrosion AASS	0.846	−0.200	1	95%

specification), and even up to 80 h without spitting corrosion initiation. All coatings with finest carbides did fail the AASS test.

4. Part II: analysis of design of experiments

All previous experimental data were collected and fed into the response matrix of the design of experiments, in order to establish relationships between process parameters (factors) and coating properties (responses). In order to describe the impact of factors onto responses, multi-linear regression (MLR) fits of the data were computed (Table 4), where R^2 describes how well the model fits the data. The model validity coefficient highlights here the presence of outliers, incorrect or transformation problem for selected response, if its value becomes lower than 0.25. The significance of the weighting coefficient of each factor and their respective interactions on the studied response, are also expressed considering the normal distribution of studentized residuals, and the replicate index, expressed through the reproducibility variable. The latest expresses the variation of the replicates compared to overall variability, and warrants a good reproducibility if greater than 0.5. Once the MLR were refitted, each response was represented as a function of the most significant factor influence, and displayed as a contour plots, with a confidence interval (C.I.) of 95%.

4.1. Relationships between powder feedstock features and coatings microstructure

As three factors were initially introduced in this design, each response is plotted as a function of the two main factors, keeping the third one with lower significance to its center level of variation. As perceived previously, the MLR model (Table 4) cannot fit the porosity response, with all coefficients becoming non-significant to explain possible variation of the porosity response in the studied design. Even if here this response is plotted as a function of PS and CGS (Fig. 6-a), the porosity level is globally kept constant and below 1% for all coatings, independently of the powder feedstock characteristics. Regarding the carbide phase content, its volume fraction likely increases with either decreasing the CGS or increasing the powder strength for small BGS (Fig. 6-b), whereas no variation was noticed with larger BGS. Regarding the carbide grain size, the trend of increasing the CGS of the introduced powder feedstock is preserved after spraying. However the absolute value of the CGS is found lower for the coated systems then the one initially introduced from the powder feedstock material (Fig. 7-a). The carbide density is found to increase while refining the carbide grain size, identically to the trend observed for the carbides contiguity and their respective density (Fig. 7-b). The influence of both the size of binder phase and the powder strength is here less significant, if not to mention that coarsening CGS and refining BGS lead to the decrease the density of both carbides and carbide–carbide interactions, while increasing their respective weighted-mean values. The increase of the coating CGS has to be related to the broadening of the weighted-distributions (Table 2), as illustrated in the next section (Fig. 8-c).

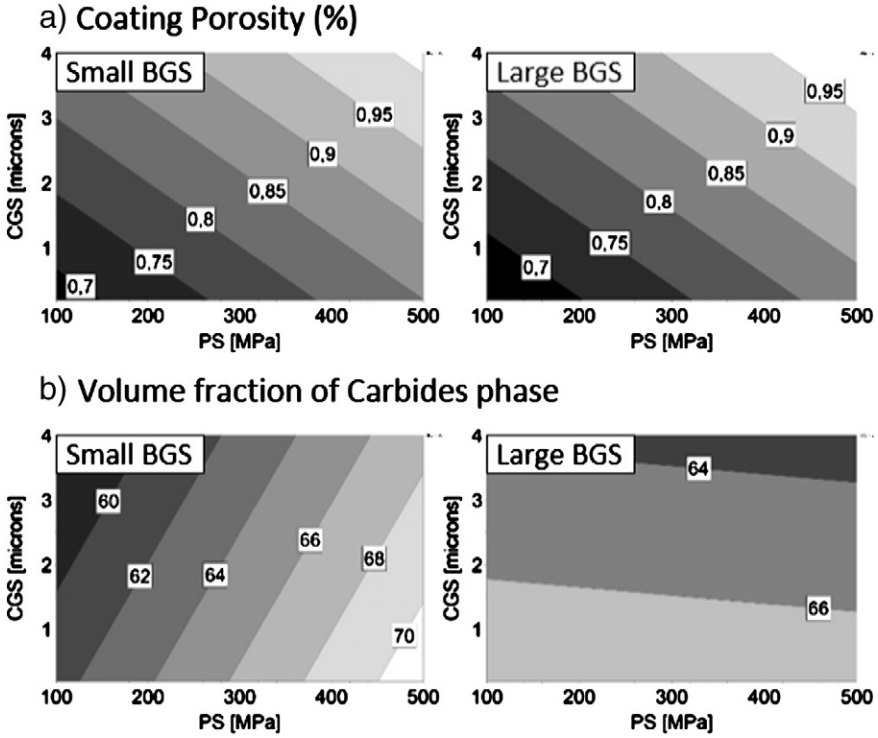

Fig. 6. Contour plots for small/large binder grain size of a) coating porosity, and b) volume fraction of carbides.

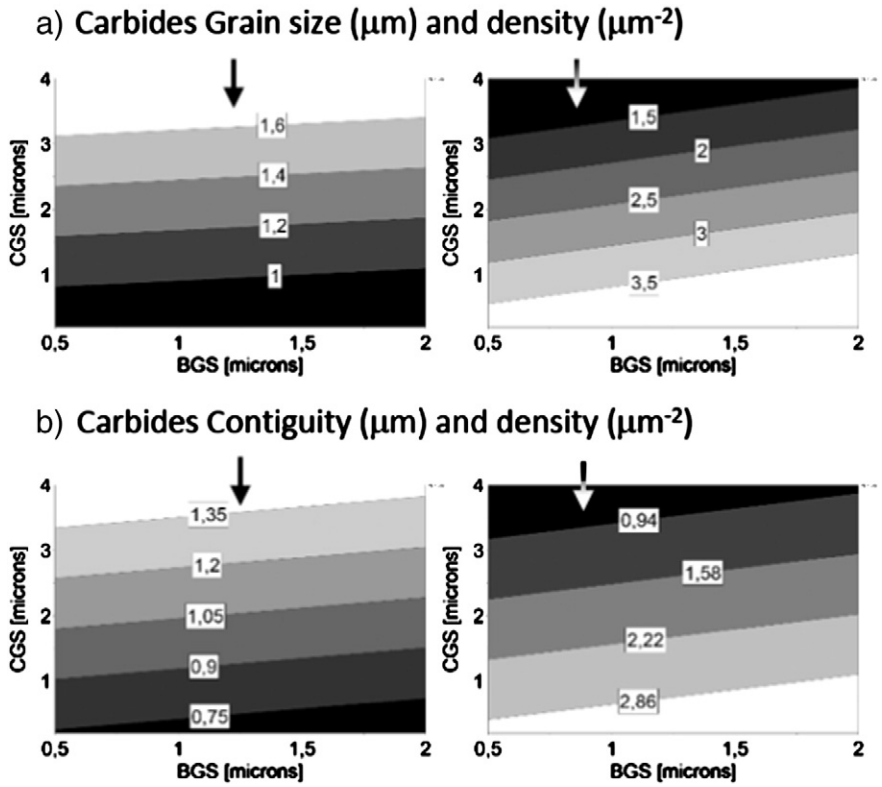

Fig. 7. Contour plots of a) coatings CGS and CGS-density, and b) coatings CC and CC-density.

4.2. Relationships between powder feedstock features and coating microhardness

Relationships between powder feedstock features and coating microhardness, carbide decarburization, and width of respective CGS and CC weighted-distributions, have been here described by MLR models (Table 4). Coefficients of linear regression (R^2) have to be considered as very high for the selected responses. Independently of the applied indentation load, all three microhardness responses exhibit the same relationship with both CGS and PS factors and their principal

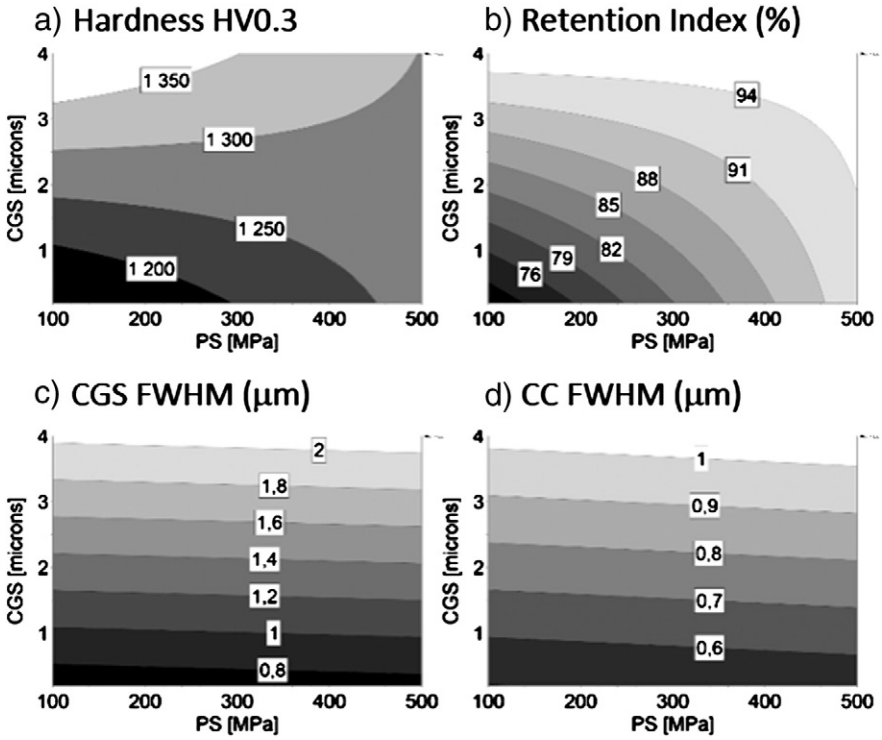

Fig. 8. Contour plots of a) microhardness HV0.3, b) respective carbide retention index, and full width at half maximum of c) CGS and d) CC weighted-distributions.

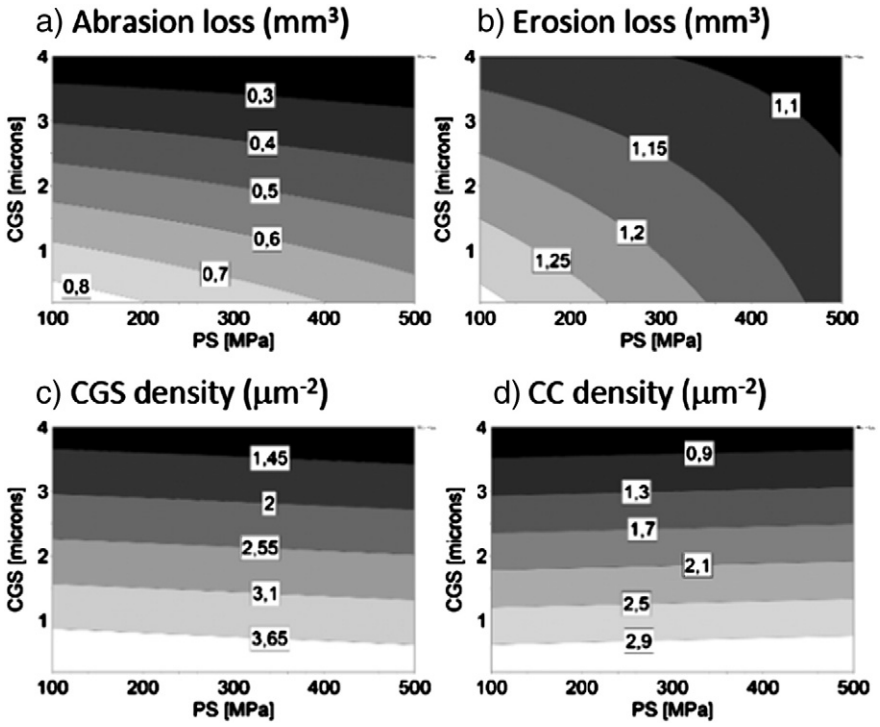

Fig. 9. Contour plots of a) abrasion and b) erosion wear loss, c) CGS density and d) CC density responses.

interaction, which is highlighted here by non-linearity in the contour plots of HV0.3 response (Fig. 8-a). Increasing both the powder strength and the primary carbide size leads to increase the coating microhardness, as well as increasing the carbides retention index (Fig. 8-b). It is here interesting to correlate the increase of the coating microhardness to the broadening of both CGS and CC weighted-distributions (Fig. 8-c–d), with the presence of fewer but coarser and less-decarburized carbides, which mostly carry the indentation information, even if the global volume fraction of carbides slightly decreases (Fig. 6-b). This could have been perceived from start as controversial, initially thinking that designing a coating with a lower volume fraction of carbides, relatively to the volume fraction of binder material, might lead to decrease its microhardness, which is not necessarily true as shown here. The information regarding the distribution and density of carbide grain size and carbide contiguity is therefore given full attention to correlate their influence on coating microhardness and wear resistance properties.

4.3. Relationships between powder feedstock features and coating wear resistance

Both abrasion and erosion volume wear loss responses exhibit a strong relationship with both the carbide grain size, the powder strength and their interaction, which could be well-described by MLR models (Table 4). As already perceived from collecting the wear raw data in Part I, the regression coefficient (R^2) was found to be higher for the abrasion response, which exhibited larger wear loss variations (Fig. 5-a), than for the erosion one (Fig. 5-b). As observed for the coating microhardness response, respective abrasion (Fig. 9-a) and erosion resistance ((Fig. 9-b) is increasing with both coarsening of the primary carbide size and increase of the powder strength. The increase of the initial powder strength has nevertheless a more pronounced effect on the erosion than on the abrasion resistance, due to the respective use of coarse erosive and fine abrasive media. Those relationships are likely due to coarsening less-decarburized carbide grains, which carry the

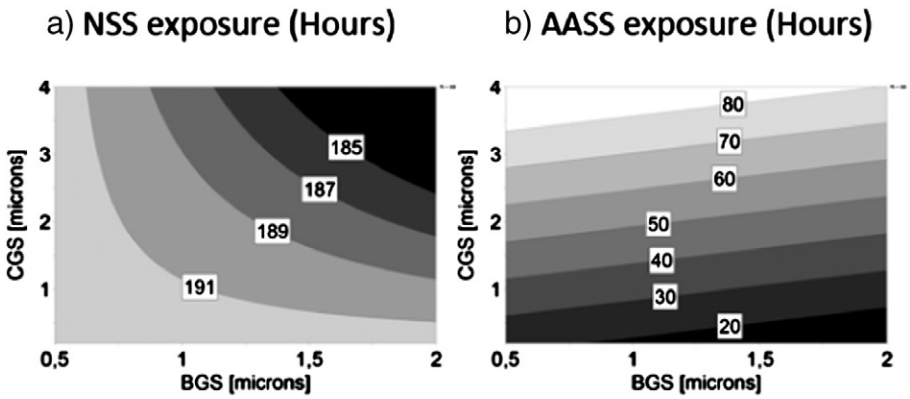

Fig. 10. Contour plots of coating corrosion resistance after exposure in a) NSS and B) AASS environments.

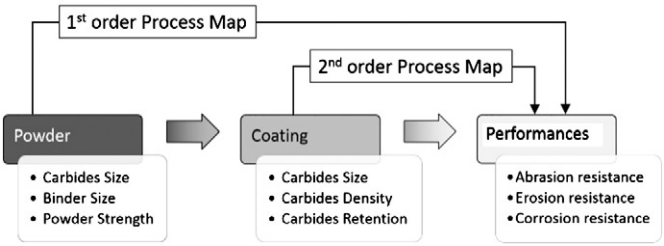

Fig. 11. First and second order process maps.

compressive abrasion and erosion wear loads (Fig. 9-c). For both wear tests, the measured volume wear loss is related to progressive loosening of carbides under severe cycling loading leading to fatigue crack propagation [10]. This phenomena of debounding between carbide phase and the surrounding binder phase is more predominant while (i) combining a high density of fine primary carbides, and (ii) combining a high density of carbides contiguity (Fig. 9-d) with finer binder grains (Fig. 7-b). Such configuration enhances carbide-to-carbide contacts instead of soliciting plastic deformation of the binder, leading to carbide grain fracture, crack initiation and propagation toward carbides debounding from the matrix.

4.4. Relationships between powder feedstock features and coating corrosion resistance

The relationship between powder features and NSS response could not be described by a MLR model, which shows very low regression coefficient and a negative validity (Table 4). However all coatings, except the one with coarser CGS, coarser BGS and highest PS, did succeed the NSS corrosion test after 192 hour exposure time, independently of the powder strength. Therefore the contour plot of the NSS response was still displayed as a function of CGS and BGS (Fig. 10-a). Whether the corresponding MLR model was not statistically relevant, it does show the trend/risk that the NSS resistance can be affected if considering both coarse CGS and coarse BGS. The corrosion resistance results to AASS environment shows significant differences (Fig. 10-b). AASS corrosion improved with coarsening the carbide grain size. Refining the binder grain size indicates a slight improvement of the global coating corrosion resistance.

4.5. Optimization and 2nd order process map

A first order process map has been established through a screening objective in order to identify relationships between powder feedstock material features and resulting coating properties (Fig. 11). Carbide grain size (CGS), binder grain size (BGS) and powder strength (PS) were selected as the factors describing the powder characteristics issued from manufacturing process. Such first order process map is therefore primordial in designing coating properties from a feedstock material point of view, in order to select powder specifications for specific coating requirements. When abrasion and erosion resistance applications are being targeted, it is also interesting to design the coating microstructural features required to offer the most adapted protection. A second order process map can therefore be established while now selecting coating microstructural features as main factors (Fig. 11), such as the carbide grain size (CGS-C), carbide grain size density (CGS-D) and the carbide retention index (I-WC). Relationships between coating microstructural features and abrasion and erosion resistance performances could be well-described by partial least square (PLS) regressions, at this point utilized to construct good predictive models. Coating abrasion resistance (Fig. 12-a) can be significantly improved (i) with coarsening the size of less-decarburized primary carbides and (ii) with increasing the density of those primary carbides. Coating erosion resistance (Fig. 12-b) is shown to be significantly improved with (i) coarsening the size of less-decarburized primary carbides, and (ii) with a decrease of their density. The coating resistance

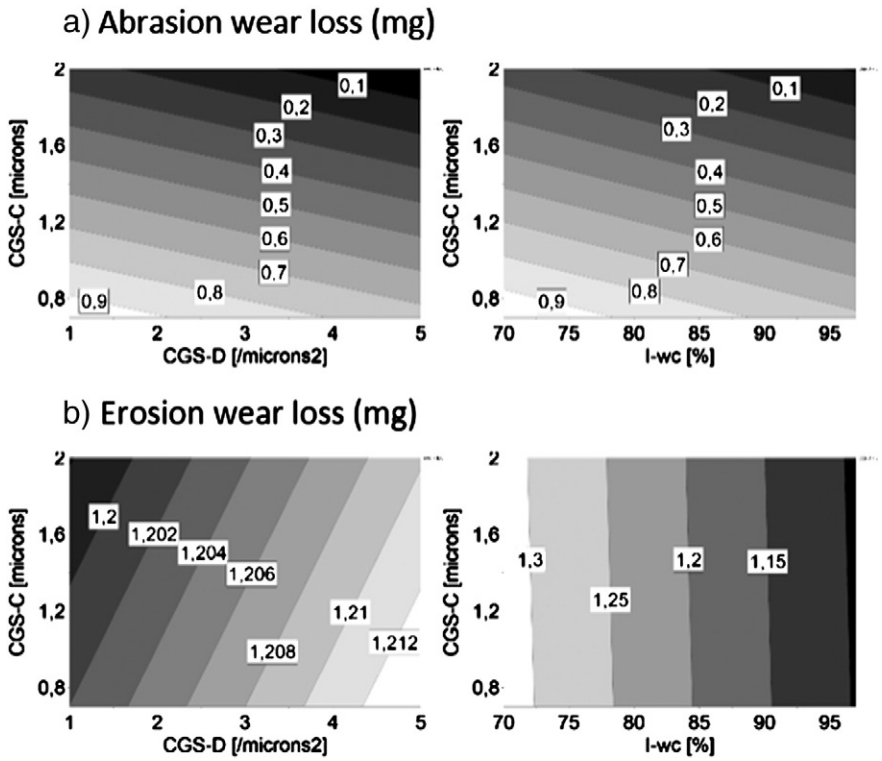

Fig. 12. Contour plots of coating A) abrasion and b) erosion wear loss—2nd order process map.

to the erosion load with coarser media, is here shown to be improved with decreasing the contact density between coarse carbides, enhancing the cohesion between the matrix material and the coarse hard phase, which mostly react to the compression and erosion mechanical loads.

5. Conclusion

Three main powder feedstock characteristics, respectively the primary carbide grain size (CGS), the binder grain size (BGS) and the powder strength (PS), have been investigated in this work, in order to highlight their respective relationships with HVAF-sprayed coatings properties. Experiments were architected through a full factorial design with screening objectives. The main results can be summarized as followed:

- Coarsening the CGS and increasing the PS of the powder feedstock lead to (i) coarsening of the resulting coating CGS, and respectively (ii) a decrease of both carbide volume fraction and carbide density. The coarser and the fewer the primary carbides, combined with finer BGS, the lower the carbide contiguity, which might give specific intrinsic mechanical properties highlighted below.
- Coating microhardness increases with coarsening the powder CGS, likely due to the presence of fewer but coarser carbides in the coating, even if the respective volume fraction of carbides decreases. The trends observed with increasing the indentation loads are more difficult to analyze, since each test is gauging an increasing volume of both matrix material and hard phases with different grain sizes. However the hardest coatings were obtained combining coarse CGS, coarse BGS and low PS. Low powder strength, if synonym of higher ductility of in-flight particles, might be here the key-parameter.
- Coarsening CGS and increasing PS of the powder lead to minimizing the primary carbide decarburization, measured by computing the relative and respective retention index from XRD patterns.
- Coating abrasion and erosion resistance increase with both coarsening the CGS and powder strength. Such CGS-based relationship has already been investigated in our previous study.
- All HVAF-sprayed coatings succeeded the NSS corrosion test, after 192 hour exposure period. Combination of coarse CGS with refined BGS leads to improve the AASS corrosion performance of the coating above 80 hour exposure time.
- Last but not least, a second order process map has been established to design the coating microstructure toward improved abrasion and erosion resistance. An identical design approach is about to be addressed regarding tribological performances of respective coated systems. Sliding wear mechanisms and friction coefficients are about to be evaluated at room and high temperature, while carrying out ball-on-disk (ASTM G99) and block-on-ring (ASTM G77) tests.

Acknowledgments

The authors would like to express their gratitude to Stefan Björklund for his help in processing, engineering and developing our HVAF thermal spray resources at the University West and Production Technology Centre in Trollhättan, Sweden.

References

[1] M. Bielewski, Replacing cadmium and chromium, Research and Technology Organisation and NATO, RTO-AG-AVT-140, 2011. 1–22 (Chp.23).
[2] K.O. Legg, Proceedings of the International Conference on Surface Modification Technologies, 15th, ASM International, Materials Park, Ohio, 2002, p. 235/244.
[3] L. Lusvarghi, G. Bolelli, T. Börner, C. Lyphout, N. Markocsan, P. Nylén, H. Koivuluoto, P. Sassatelli, P. Vuoristo, S. Zimmermann, L.M. Berger, World Tribology Conference, Torino, Italy, 2013.
[4] P.H. Shipway, D.G. McCartney, T. Sudaprasert, Wear 259 (2005) 820–827.
[5] Q. Yang, T. Senda, A. Ohmori, Wear 254 (2003) 23–34.
[6] G. Bolelli, L.M. Berger, M. Bonetti, L. Lusvarghi, Wear 309 (2014) 96–111.
[7] C. Bartuli, T. Valente, F. Cipri, E. Bemporad, M. Tului, J. Therm. Spray Technol. 14 (2005) 187–195.
[8] C.-J. Li, G.-J. Yang, Int. J. Refract. Met. Hard Mater. 39 (2013) 2–17.
[9] S.L. Liu, X.P. Zheng, G.Q. Geng, Wear 269 (2010) 362–367.
[10] A.D. Pogrebnjak, M.V. Il'yashenko, V.S. Kshnyakin, et al., Tech. Phys. Lett. 27 (9) (2001) 749–752.
[11] F.D. Witherspoon, D.W. Massey, R.W. Kincald, G.C. Whichard, T.A. Mozhi, J. Therm. Spray Technol. 11 (1) (2002) 119–128.
[12] Q. Wang, S. Zhang, Y. Cheng, J. Xiang, X. Zhao, G. Yang, Surf. Coat. Technol. 218 (2013) 127–136.
[13] L. Jacobs, M.M. Hyland, M.D. Bonte, J. Therm. Spray Technol. 7 (2) (1998) 213–218.
[14] L. Jacobs, M.M. Hyland, M.D. Bonte, J. Therm. Spray Technol. 8 (1) (1999) 125–132.
[15] C. Lyphout, J. Kitamura, K. Sato, S. Dizdar, Thermal Spray, in: R.S. Lima, A. Agarwal, M. M. Hyland, Y.-C. Lau, G. Mauer, A. McDonald, F.-L. Toma (Eds.), Proceedings of the International Thermal Spray Conference, May 13–15, 2013, Busan, South Korea.
[16] C. Lyphout, K. Sato, ITSC, 2014, ASM International, (Barcelona, Spain).
[17] C.J. Li, Y.Y. Wang, G.J. Yang, A. Ohmori, K.A. Khor, Mater. Sci. Technol. 20 (2004) 1087–1096.